# High-$T_c$ superconducting materials for electric power applications

**David Larbalestier, Alex Gurevich, D. Matthew Feldmann & Anatoly Polyanskii**

*Applied Superconductivity Center, Department of Materials Science and Engineering, Department of Physics, University of Wisconsin, Madison, Wisconsin 53706 USA (e-mail: larbalestier@engr.wisc.edu)*

**Large-scale superconducting electric devices for power industry depend critically on wires with high critical current densities at temperatures where cryogenic losses are tolerable. This restricts choice to two high-temperature cuprate superconductors, $(Bi,Pb)_2Sr_2Ca_2Cu_3O_x$ and $YBa_2Cu_3O_x$, and possibly to $MgB_2$, recently discovered to superconduct at 39 K. Crystal structure and material anisotropy place fundamental restrictions on their properties, especially in polycrystalline form. So far, power applications have followed a largely empirical, twin-track approach of conductor development and construction of prototype devices. The feasibility of superconducting power cables, magnetic energy-storage devices, transformers, fault current limiters and motors, largely using $(Bi,Pb)_2Sr_2Ca_2Cu_3O_x$ conductor, is proven. Widespread applications now depend significantly on cost-effective resolution of fundamental materials and fabrication issues, which control the production of low-cost, high-performance conductors of these remarkable compounds.**

The potential applications of superconductors — Kamerlingh Onnes's name for materials that lose electric resistance on cooling below a transition temperature, $T_c$ — were apparent to Onnes almost immediately. In 1913, just two years after his discovery, Onnes talked in Chicago about the design of very powerful magnets far exceeding the fields achievable by iron; these would cost as much as a battleship if made from copper and cooled with liquid air, but be affordable if made from superconducting wires. By that time he had already tested a Ni alloy coated with Pb-rich superconducting solder, but this lost superconductivity at fields of less than 50 mT. He ascribed this unexpected setback to bad places in the wire, a problem he anticipated would soon be fixed without difficulty!

In fact, applications had to wait 50 more years, particularly because the physics of superconductivity in magnetic fields were seriously misunderstood[1]. This need not have been so, because London and Shubnikov made important breakthroughs in understanding the magnetic properties of superconductors in the 1930s. By careful alloying experiments, Shubnikov pointed out the vital distinction between type I superconductors, in which currents flow only at the surface and superconductivity is destroyed by weak fields, as in Onnes' 1913 experiment, and a new type of super conductor, now called a type II superconductor, capable of carrying bulk supercurrent at high fields. The key understanding that the behaviour of type II superconductors is due to quantized magnetic vortices was achieved by Abrikosov in the 1950s.

In spite of these theoretical insights, it was not until 1961 that Kunzler *et al.*[2] showed that high-field applications really were possible. Drawing Sn inside a Nb wire and reacting it to form the brittle intermetallic $Nb_3Sn$, they reached a current density $J > 10^5$ A cm$^{-2}$ at 8.8 T and 4.2 K. This astounding result demonstrated that superconductivity could indeed exist in very high magnetic fields. In fact, Onnes's vision for a 10 T, high-field magnet has been abundantly fulfilled. Laboratory superconducting magnets exist by their thousands, some producing fields exceeding 20 T. Fermilab, Brookhaven, DESY and CERN all have accelerators composed of kilometres of superconducting bending and focusing magnets (see, for example, the proceedings of the biennial Applied Superconductivity Conferences published in odd-year volumes of *IEEE Trans. Magn.* up to 1989, and *IEEE Trans. Appl. Supercond.* since 1991). The medical technique of magnetic resonance imaging was developed using very homogeneous, persistent-mode superconducting magnets, a business now exceeding US$3 billion per year.

All of these applications are based on two low-temperature superconducting (LTS) materials, Nb-Ti alloy ($T_c = 9$ K) or $Nb_3Sn$ ($T_c = 18$ K). For such applications, superconductivity is a true enabling technology and the use of liquid helium or helium-driven refrigerators is immaterial. But helium cooling tends to be too expensive for replacement of conventional electrotechnology based on Cu and Fe, two cheap and well understood materials. The first period of superconducting applications, from approximately 1962 to 1986, explored various power applications but found them too complex and expensive, thus relegating superconductivity to new high-technology and medical applications where no competitors existed. By 1986, the highest-$T_c$ compounds possessed the A15 structure, the lightest of which, $Nb_3Ge$, has a $T_c$ of 23 K (ref. 3), 5-K higher than for $Nb_3Sn$.

Prospects changed dramatically in late 1986, when Bednorz and Muller[4] discovered superconductivity at 30 K in the layered cuprate, $LaBa_2CuO_{4-x}$. In early 1987, superconductivity in $YBa_2Cu_3O_x$ (YBCO) at 92 K was announced[5], well above the boiling point of liquid nitrogen (77 K). Soon $T_c$ rose to more than 130 K (ref. 6) in $Hg_2Ba_2Ca_2Cu_3O_x$. Widespread replacement of Cu and Fe by these new high-temperature superconductors (HTSs) was broadly discussed and significant public and private programmes to build electric utility superconducting devices were put in place in Japan, Europe and the United States[7]. Major components of the generation, transmission (power cables and devices for superconducting magnetic energy storage), distribution (transformers and fault current limiters) and end-use (motor) devices have been built, primarily using the $(Bi,Pb)_2Sr_2Ca_2Cu_3O_x$ (Bi-2223) conductor[7].

Superconductivity can have a significant role in deregulated electricity markets and in lessening $CO_2$ emissions and

other environmental impacts, but significant market penetration of HTS devices requires HTS wires that fully exploit their fundamental current-carrying capability. The announcement by Akimitsu in January 2001 that the binary compound $MgB_2$ superconducts at up to 39 K (ref. 8) has generated new interest in superconductors for power applications, owing to the cheap abundance of Mg and B and the potential of analogous compounds.

## Conductor requirements for power technology

A conductor is more than just the superconductor. Conductors for power applications are multifilamentary wires or tapes in which many superconducting filaments are embedded in a matrix of a normal metal, such as Cu or Ag, which provides protection against magnetic flux jumps and thermal quenching[9] (Fig. 1). Such wires must have sufficient strength to withstand the fabrication process, device winding, cool-down and electromagnetic stresses, and be capable of being made or cabled to sufficient size to carry operating currents from hundreds to thousands of amperes at costs comparable to Cu. Estimates of the acceptable cost range from about US$10 to US$100 per kA m, the scale being set at its lower end by the cost for Cu (~$US15 per kA m) and at the upper end by higher-cost applications where superconductivity has advantages not possessed by present technology[7,10]. Such higher-cost applications include high power density underground power cables in inner cities, environmentally friendly, oil-free HTS transformers, or superconducting magnetic energy-storage devices for power networks where low reactance and instantaneous redistribution of power is vital[11].

These requirements define a parameter set that restricts present choice to Bi-2223 or YBCO. The combination of critical current density $J_c$, field and operating temperature is summarized in Table 1. Target superconductor current densities must attain $10^4$–$10^5$ A cm$^{-2}$ in fields of 0.1–10 T at temperatures of 20–77 K. The data in Table 1 represent an ongoing dialogue between the R&D and applied communities that tends to push up the operating temperature, current density and field so as to better separate a Cu and Fe technology limited to fields of 1–2 T from a higher-field, superconductor-based technology. Reliable and inexpensive refrigeration is a critical part of the HTS technology and significant advances have been made in this area too[12].

At present, the only HTS conductor in production is Ag-sheathed Bi-2223 with $T_c$ ~108 K (its lower-$T_c$ sibling $Bi_2Sr_2CaCu_2O_x$ has only a small application in the power sector). Figure 1 shows a cross-section of a Bi-2223 conductor of the type being used for the Detroit Edison 100-MVA power cable, in which multiple strands are wound to make a fully transposed 6,000-A cable operating at 70–75 K. The individual strand is 0.2 mm by 4 mm with a critical current $I_c$ of the order of 125 A in zero field at 77 K. Underpinning conductor R&D programmes worldwide is the conviction that such conductors have neither the magnetic field performance for applications at liquid nitrogen temperatures (~65–80 K), nor sufficiently low costs. The potential lower-cost alternative is a biaxially textured YBCO conductor or possibly $MgB_2$ or an analogous compound[13]. We now explore the underlying materials issues that define these beliefs.

## Superconducting properties, crystal structure and anisotropy

Figure 2 presents the important magnetic field–temperature ($H$–$T$) phase diagram for the three actual (Nb-Ti, $Nb_3Sn$ and Bi-2223) and two potential (YBCO and $MgB_2$) conductor materials. Their different phase diagrams result from their distinctly different physical parameters and crystal structures, as shown in Fig. 3 and Table 2. All five are type II superconductors for which bulk superconductivity exists up to an upper critical field $H_{c2}(T)$, which can exceed 100 T for Bi-2223 and YBCO. In fact, applications are limited by a lower characteristic field, the irreversibility field $H^*(T)$ at which $J_c$ vanishes. For the isotropic cubic superconductors, Nb-Ti and $Nb_3Sn$, $H^*(T)$ is about $0.85H_{c2}(T)$ (refs 14,15). All three higher-$T_c$ compounds have anisotropic layered structures, which result in significant anisotropy of the upper critical field, $\eta = H_{c2}^{\parallel}(T)/H_{c2}^{\perp}(T)$, parallel and perpendicular to the superconducting layers. Here $\eta$ has values of 1 for Nb-Ti and $Nb_3Sn$, 2–3 for $MgB_2$ (refs 16,17), 5–7 for YBCO, and

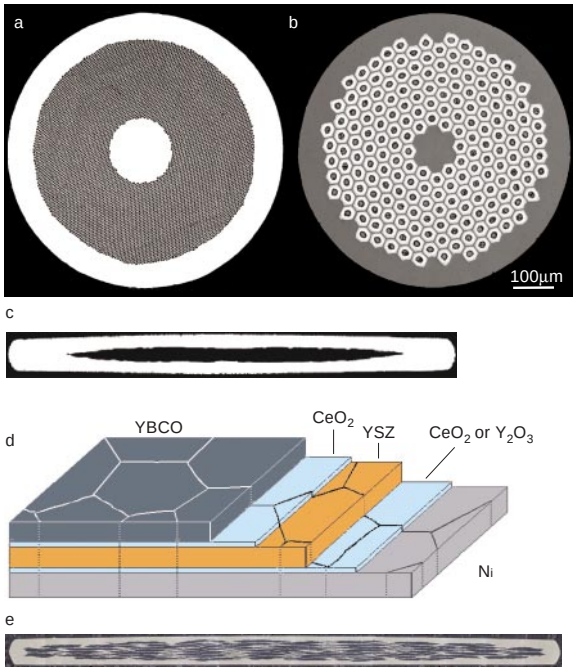


**Figure 1** Conductor forms of practical superconductors. **a**, Conductor containing about 3,000 Nb47wt%Ti filaments embedded in a copper stabilizer, which protects the conductors during a transition (quench) to the normal state. The wire is ~0.8 mm in diameter and the filament diameter is 10 μm. **b**, Powder-in-tube $Nb_3Sn$ conductor made by extruding and drawing a mixture of $NbSn_2$ and Cu inside the Nb tubes that form each of the 192 filaments. The conductor is ~1 mm in diameter and the filaments are ~20 μm in diameter. **c**, Cu-sheathed $MgB_2$ tape made by rolling $MgB_2$ powder in a copper tube. The tape is ~0.2 mm thick by 4 mm wide[80]. **d**, Structure of a deformation-textured coated conductor. Typical thicknesses of the Ni, $CeO_2/Y_2O_3$, YSZ, $CeO_2$ and $YBa_2Cu_3O_x$ (YBCO) layers are (respectively) 50–100 μm, 10 nm, 300 nm, 10 nm and 0.3–2 μm. **e**, Cross-section of a 55-filament $(Bi,Pb)_2Sr_2Ca_2Cu_3O_x$ (Bi-2223)-power cable tape encased in a silver matrix, which acts as stabilizer. The tape is ~0.2 × 4 mm wide. All conductors except the coated conductor were made by conventional extrusion, wire drawing and/or rolling techniques.

**Table 1 Industry consensus wire performance requirements for various utility device applications**

| Application | $J_c$ (A cm$^{-2}$) | Field (T) | Temperature (K) | $I_c$ (A) | Wire length (m) | Strain (%) | Bend radius (m) | Cost (US$ per kA m) |
|---|---|---|---|---|---|---|---|---|
| Fault current limiter | $10^4$–$10^5$ | 0.1–3 | 20–77 | $10^3$–$10^4$ | 1,000 | 0.2 | 0.1 | 10–100 |
| Large motor | $10^5$ | 4-5 | 20–77 | 500 | 1,000 | 0.2–0.3 | 0.05 | 10 |
| Generator | $10^5$ | 4–5 | 20–50 | >1,000 | 1,000 | 0.2 | 0.1 | 10 |
| SMES* | $10^5$ | 5–10 | 20–77 | ~$10^4$ | 1,000 | 0.2 | 1 | 10 |
| Transmission cable | $10^4$–$10^5$ | <0.2 | 65–77 | 100 per strand | 100 | 0.4 | 2 (cable) | 10–100 |
| Transformer | $10^5$ | 0.1–0.5 | 65–77 | $10^2$–$10^3$ | 1,000 | 0.2 | 1 | <10 |

*SMES, superconducting magnetic-energy storage.
Data supplied by R. Blaugher.

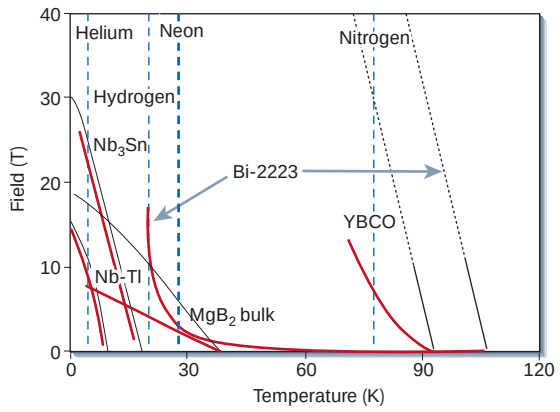


**Figure 2** Magnetic field–temperature diagram for Nb47wt%Ti, $Nb_3Sn$, $MgB_2$, Bi-2223 and YBCO. The upper critical field $H_{c2}$ at which bulk superconductivity is destroyed is indicated in black, while the irreversibility field $H^*$ at which the bulk critical current density goes to zero is indicated in red. It can be seen that $H^*(T)$ is close to $H_{c2}(T)$ for Nb-Ti and $Nb_3Sn$, about half of $H_{c2}(T)$ for $MgB_2$, and much lower than $H^*(T)$ for YBCO and Bi-2223. There is not much scope for using Bi-2223 at 77 K because its irreversibility field (~0.3 T) is so low. As a result, applications at 77 K are restricted mostly to power cables for which the self-field is well below $H^*$(77K).

50–200 for Bi-2223 (ref. 18). In all cases, $H_{c2}$ and $H^*$ are lower for field applied parallel to the *c*-axis and perpendicular to the *a*–*b* planes. Figure 2 shows that strongly anisotropic Bi-2223 exhibits an enormous suppression of $H^*$(77K) to the very low value of ~0.2 T, well below $H_{c2}$(77K), which is of order 50 T for $H$ parallel to the *c*-axis[19]. This low irreversibility field prevents use of Bi-2223 at 77 K in any significant field (although power cables are possible) and provides one of the key arguments for developing a second-generation HTS technology based on YBCO, for which $H^*(77K) \sim 7$ T.

The structural origin of these important superconducting anisotropies is illustrated in Fig. 3 and Table 2. Nb-Ti, normally Nb47-50wt%Ti, is a body-centred cubic, solid-solution alloy with short electron mean-free-path, high resistivity and coherence length $\xi(4K) = 5$ nm. $Nb_3Sn$ has $\xi(4K) = 3$ nm and possesses the cubic A15 crystal structure, in which three orthogonal chains of Nb atoms separate the Sn atoms lying at cube corners and cube centre. $MgB_2$ has the hexagonal space group *P*6/*mmm* composed of alternating B and Mg sheets, the B being nested in the Mg interstices[8]. It can form as a low-resistivity ($\rho(40K) = 0.4$ μΩ cm), perhaps perfectly stoichiometric compound[20] for which $\xi(4K)^{\perp} = 6.5$ nm and $\xi(4K)^{\parallel} = 2.5$ nm, where the perpendicular direction along the *c*-axis is taken with respect to the B planes in $MgB_2$ and the $CuO_2$ planes in HTSs. YBCO is a complex, layered perovskite centred on a Y layer, around which are stacked the $CuO_2$ plane of strong superconductivity and a double charge-reservoir layer of O-Ba-O and O-Cu. In Bi-2223, the charge-reservoir layer consists of a double (Bi,Pb)-O and its neighbouring Sr-O layers, the superconducting layers being a stack of three $CuO_2$ layers interleaved by two Ca layers. The anisotropy of Bi-2223 is so large that $H^*$(77K) is only 0.2–0.3 T, restricting 77-K applications to low self-field uses such as power cables, even though $H_{c2}$(77K) exceeds 10 T.

## Flux pinning and the critical current density

Under equilibrium conditions, magnetic flux penetrates the bulk of a type II superconductor above the lower critical field $H_{c1}$, which is of order 10-20 mT for the materials under consideration. Over most of the available $H$–$T$ space, $H > H_{c1}$, this magnetic flux exists as a lattice of quantized line vortices or fluxons[18,21]. Each fluxon is a tube of radius of the London penetration depth $\lambda(T)$, in which superconducting screening currents circulate around a small non-superconducting core of radius $\xi(T)$, where $\xi(T)$ is the superconducting coherence length. The flux carried by the screening currents in each fluxon equals the flux quantum $\phi_0 = 2 \times 10^{-15}$ Wb. Bulk superconductivity is destroyed when the normal cores overlap at the upper critical field, $H_{c2}(T) = \phi_0/2\pi\mu_0\xi(T)^2$. In isotropic materials such as Nb-Ti and $Nb_3Sn$, vortex lines are continuous, but the weak superconductivity of the blocking layers of HTS compounds produces a stack of weakly coupled 'pancake' vortices whose circulating screening currents are mostly confined within the superconducting $CuO_2$ planes[18].

Superconductors can carry bulk current density only if there is a macroscopic fluxon density gradient[22], defined by the Maxwell equation $\nabla \times \mathbf{B} = \mu_0 \mathbf{J}$. This gradient can be sustained only by pinning the vortices (flux pinning) at microstructural defects. Increasing $T$ and $H$ weaken the potential wells at which vortices are pinned, thus lessening $H^*(T)$ and $J_c(T,H)$. Flux pinning is determined by spatial perturbations of the free energy of the vortex lines due to local interactions of their normal cores and screening currents with these microstructural imperfections[22]. In addition, the fluxon structure is subjected to the Lorentz force $\mathbf{F}_L = \mathbf{J} \times \mathbf{B}$ of the macroscopic current. The critical current density $J_c(T,H)$ is then defined by the balance of the pinning and Lorentz forces, $F_p = F_L$, where $F_p$ is the volume summation over all microstructural pinning defects in the strongly interacting network of flux lines. Ideally, a type II superconductor can carry any non-dissipative current density $J$ smaller than $J_c$. When $J$ exceeds $J_c$, a superconductor switches into a dissipative, vortex-flow state driven by the Lorentz force.

This description of flux pinning immediately suggests tailoring the defect structure of the conductor to maximize $J_c$. In fact, this does not correspond well to the essentially empirical way in which conductors have been developed, especially those of Bi-2223 and YBCO, for which the important flux-pinning defects are largely unknown. In practice, it is the critical current $I_c$ of a wire of cross-section $A$ that is measured, normally at the finite electric field of 1 μV cm$^{-1}$. The physics of vortex dynamics and pinning is enormously interesting[18,22], but equally important in practical terms is the fact that the actual cross-section over which transport currents flow in HTS conductors is much less than the whole[23]. What has greatly held back the development of Bi-2223 conductors in particular is uncertainty about whether the long-range utilization of the current-carrying cross-section of state-of-the-art conductors is 5, 25 or 50%. It is certain that it is not 100%, for reasons discussed later. Irrespective of such percolative current-flow effects, the upper limit to the critical current is set by

**Table 2 Basic material and critical current density relevant parameters for practical superconductors**

| Material | Crystal structure | Anisotropy | $T_c$ (K) | $H_{c2}$ | $H^*$ | In-plane coherence length $\xi(0)$ (nm) | In-plane penetration depth $\lambda(0)$ (nm) | Depairing current density (A cm$^{-2}$), 4.2 K | Critical current density (A cm$^{-2}$) | $\rho(T_c)$ (μΩ cm) |
|---|---|---|---|---|---|---|---|---|---|---|
| Nb47wt%Ti | Body-centred cubic | Negligible | 9 | 12 T (4 K) | 10.5 T (4 K) | 4 | 240 | $3.6 \times 10^7$ | $4 \times 10^5$ (5 T) | 60 |
| $Nb_3Sn$ | A15 cubic | Negligible | 18 | 27 T (4 K) | 24 T (4 K) | 3 | 65 | $7.7 \times 10^8$ | ~$10^6$ | 5 |
| $MgB_2$ | *P*6/*mmm* hexagonal | 2–2.7 | 39 | 15 T (4 K) | 8 T (4 K) | 6.5 | 140 | $7.7 \times 10^7$ | ~$10^6$ | 0.4 |
| YBCO | Orthorhombic layered perovskite | 7 | 92 | >100 T (4 K) | 5–7 T (77 K) | 1.5 | 150 | $3 \times 10^8$ | ~$10^7$ | ~40–60 |
| Bi-2223 | Tetragonal layered perovskite | ~50–100 | 108 | >100 T (4 K) | ~0.2 T (77 K) | 1.5 | 150 | $3 \times 10^8$ | ~$10^6$ | ~150–800 |

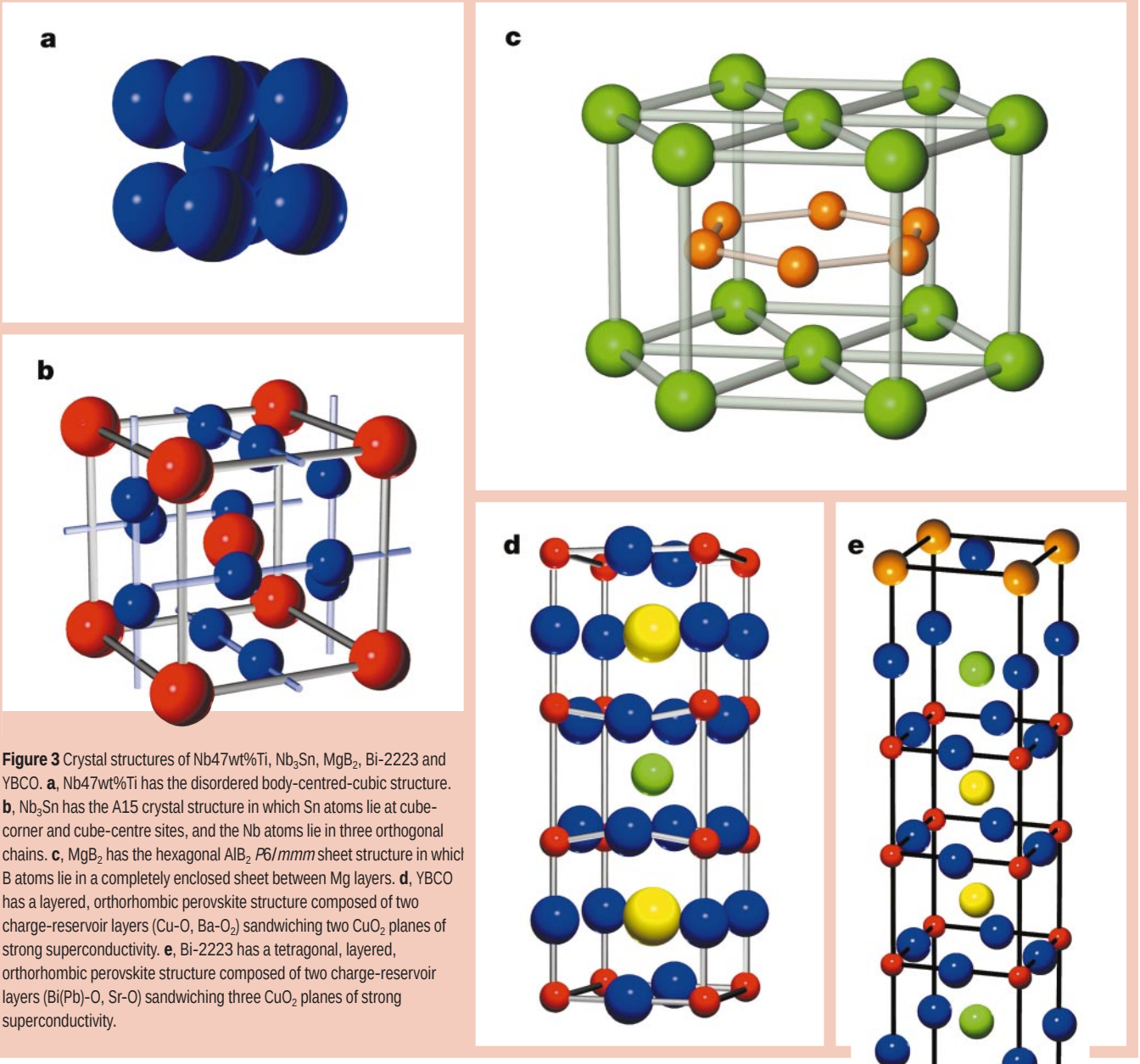


**Figure 3** Crystal structures of Nb47wt%Ti, $Nb_3Sn$, $MgB_2$, Bi-2223 and YBCO. **a**, Nb47wt%Ti has the disordered body-centred-cubic structure. **b**, $Nb_3Sn$ has the A15 crystal structure in which Sn atoms lie at cube-corner and cube-centre sites, and the Nb atoms lie in three orthogonal chains. **c**, $MgB_2$ has the hexagonal $AlB_2$ *P6/mmm* sheet structure in which B atoms lie in a completely enclosed sheet between Mg layers. **d**, YBCO has a layered, orthorhombic perovskite structure composed of two charge-reservoir layers (Cu-O, Ba-$O_2$) sandwiching two $CuO_2$ planes of strong superconductivity. **e**, Bi-2223 has a tetragonal, layered, orthorhombic perovskite structure composed of two charge-reservoir layers (Bi(Pb)-O, Sr-O) sandwiching three $CuO_2$ planes of strong superconductivity.

the flux-pinning current density, which cannot exceed the depairing current density $J_d = \phi_0/[3/(\sqrt{3})\pi\mu_0\lambda^2(T)\xi(T)]$, the maximum supercurrent density circulating near the vortex cores.

The best information that we possess about the limits to flux pinning in practical superconductors has come from extensive studies of Nb-Ti[24]. Exceptionally strong pinning by a dense, ~20–25-vol% lamellar structure of normal (that is, non-superconducting) α-Ti ribbons, about 1 nm (0.2$\xi$) thick and aligned parallel to the wire transport current, can produce a $J_c$ that approaches 5–10% of $J_d$ at zero field and 4.2 K. The flux-pinning mechanism is also known for $Nb_3Sn$, in which $J_c$ is determined by the magnetic interaction of the fluxon currents with grain boundaries[25,26]. In this case, $J_c(T,H)$ increases with decreasing grain size, thus encouraging low-temperature methods of phase formation that produce a fine grain size[27]. There are also indications of grain-boundary pinning in $MgB_2$ (refs 28–30). All three materials possess zero-field $J_c$ values, which can exceed 1 MA $cm^{-2}$ at 4.2 K.

The important flux-pinning interactions in conductor forms of YBCO and Bi-2223 are largely unknown, partly because the coherence length is so small that even atomic-sized point defects can pin fluxons. The critical temperature of HTSs is extremely sensitive to the carrier (hole) density, which is in turn determined by local oxygen (and other) non-stoichiometries, so that even a weak hole-depletion at crystalline defects can locally drive an HTS into an antiferromagnetic insulator. The proximity of the superconducting state to the metal–insulator transition, the d-wave pairing symmetry, the very short in-plane coherence length ($\xi(0) = 1.5$–2 nm) and the much longer Debye screening length ($l_D \sim \xi(0)$) all combine to produce significant suppression of the superconducting order parameter $\Delta(\mathbf{r})$ near crystal defects such as impurities, dislocations and grain boundaries[31], thus making them effective pinning centres. In fact, recent scanning tunnelling microscopy of Bi-2212 single crystals[32] has revealed significant variations of $\Delta(\mathbf{r})$ near single-atom impurities (Zn and Ni), as well as striking intrinsic variations of $\Delta(\mathbf{r})$ on scales of 1–2 nm even in pure crystals[33].

This extreme sensitivity of HTSs to nanoscale defects, along with the intrinsic spatial fluctuations of $\Delta(\mathbf{r})$ from 25 meV to 60 meV on the scale of $\xi$ or less[33], provide effective core pinning of vortices. There is strong experimental evidence that point defects such as Zn and Ni impurities[32] or oxygen vacancies[34], or line defects such as edge[35] and

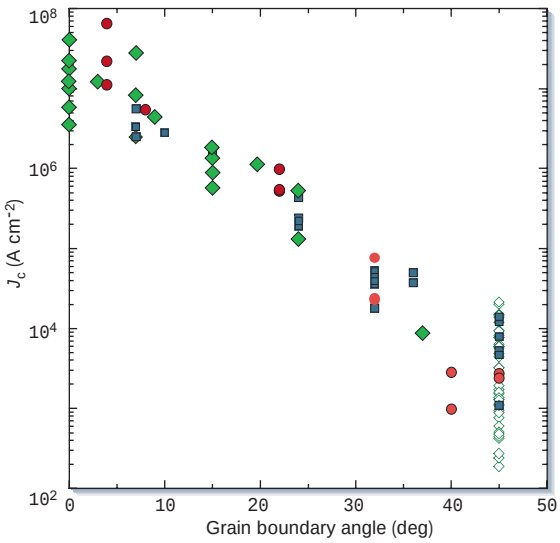


**Figure 4** Transport critical current density at 4.2 K measured in thin films of YBCO grown on [001] tilt bicrystal substrates of $SrTiO_3$ (squares[37] and filled diamonds[44]), $Y_2O_3$-stabilized $ZrO_2$ (circles[97]), and bi-epitaxial junctions (open diamonds[98]) of varying misorientation angle $\theta$. Data of refs 97 and 44 were taken at 77 K and have been multiplied by a factor of 10.9 to make them comparable with the data at 4.2 K. Despite a significant scattering, $J_c(\theta)$ exhibits a universal exponential dependence on $\theta$. Data compilation courtesy of J. Mannhart[37].

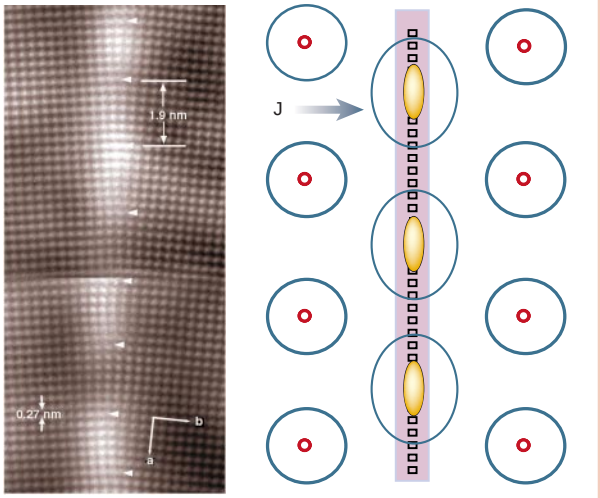


**Figure 5** Grain boundary structure and its effect on vortex properties. The left panel is a Fourier-filtered transmission electron micrograph of an 8° [001] tilt $Bi_2Sr_2CaCu_2O_x$ bicrystal, showing the edge dislocation structure at the grain boundary and the channels of good conduction that lie between their cores. Stacking faults are indicated by the white regions between alternate pairs of dislocations. Strong strains are found at the core of each dislocation. On the right is a schematic illustration of the consequences of the dislocation structure for vortices at the boundary. Abrikosov vortices are indicated within the grains, but their cores become elongated when they sit at the boundary, owing to the reduced current transparency of the boundary. The grain-boundary dislocations are indicated by the black squares and the carrier-depleted zone by the pink-shaded region. Vortices at the grain boundary acquire a mixed Abrikosov–Josephson character, which strongly reduces their pinning force along the boundary.

screw[36] dislocations, can effectively pin pancake vortices in layered HTSs. Thus, all forms of HTSs possess crystalline defects of different kinds, which provide strong flux pinning at low temperatures. Consistent with this, YBCO and Bi-2223 films[37,38] can exhibit $J_c$(4K) values of more than 10 MA cm$^{-2}$ and single crystals of YBCO (ref. 39) can exhibit values up to 1 MA cm$^{-2}$. Although these $J_c$ values are about an order of magnitude lower at 77 K, they are more than sufficient for power applications (Table 1). Moreover, they are still much lower than the depairing limit: $J_d \approx 300$ MA cm$^{-2}$ at 4 K for characteristic values $\lambda(0) \approx 150$ nm and $\xi(0) \approx 1.5$ nm. Thus, unlike Nb-Ti where the material is rather close to its performance limit, there is enormous untapped potential for improved HTS material performance.

The main obstacle for HTS conductors is that their current-carrying capability deteriorates rapidly with increasing temperature and magnetic field. As shown in Fig. 2, $J_c$ vanishes at the irreversibility field $H^*(T)$, which is far below $H_{c2}(T)$ at 77 K. An independent, significant limit on $J_c$ is current blockage by grain boundaries, as described in the next section. But the underlying cause of the suppression of $H^*(T)$ at higher temperatures is due to the layered structure of HTSs, which greatly facilitates depinning of stacks of weakly coupled pancake vortices by thermal fluctuations[15,18]. For $H < H^*(T)$, vortex fluctuations cause thermally activated creep of magnetic flux[40], producing measurable dissipation well below $J_c$ defined at 1 μV cm$^{-1}$. Anisotropy strongly enhances the effect of thermal vortex fluctuations[18], thus suppressing $H^*$ and enhancing flux creep in Bi-2223 much more than in YBCO. Both $H^*$ and $J_c$ can be significantly improved by irradiation, which creates effective columnar pinning tracks[41]. For example, neutron irradiation of U-doped Bi-2223 tapes fissions the U and produces heavy-ion tracks that raise $H^*$(77K) to over 1 T, while also reducing the anisotropy of $J_c$ (ref. 42).

## Grain boundaries

Large devices need kilometres of polycrystalline conductors and the influence of grain boundaries is therefore critical. The most unambiguous evidence that grain boundaries are strong barriers to current flow in HTSs comes from detailed studies of [001] tilt YBCO bicrystals on $SrTiO_3$ or $Y_2O_3$-stabilized $ZrO_2$ (YSZ) substrates. These have shown that the critical current density $J_b$ across the grain boundary drops exponentially below that of the grains, $J_b = J_0 \exp(-\theta/\theta_c)$, as a function of the misorientation angle $\theta$ between the neighbouring crystallites[37,43–45], where $\theta_c \approx 2$–5°, depending on the value of the intragrain $J_c$ (Fig. 4). This extreme sensitivity to misorientation, coupled with the intrinsic anisotropy of the HTS compounds, dictates the need to texture conductors into the tape forms shown in Fig. 1, so as to shift the grain-boundary misorientation distribution to as small a value of $\theta$ as possible. For Bi-2223, the rolling deformation used to make the tape produces a marked uniaxial, *c*-axis texture, whereas for YBCO-coated conductors, the essential goal is to make both in- and out-of-plane texture so that the tape behaves as a quasi-single crystal, even though the YBCO grain size is <1 μm in diameter[46,47].

This behaviour of HTS materials is in strong contrast to metallic LTS and $MgB_2$, in which grain boundaries are not only transparent to current, but also significantly contribute to flux pinning, increasing the overall $J_c$ as the grain size decreases[26,28,48]. Although Table 2 might suggest that HTS grain boundaries are weak links because of their short coherence length, in fact a value of $\xi$(77K) of ~4 nm for YBCO is actually longer than for $Nb_3Sn$ at 4 K. Moreover, low carrier density makes grain boundaries in (Ba,Pb)$BiO_3$ also weak-linked, even though $\xi$(4K) ~ 7 nm for this compound[49,50]. In fact, the weak-link (that is, current-obstructing) behaviour of grain boundaries in HTSs results from the same factors, which otherwise enhance the pinning of vortices by point defects, namely the strong dependence of $T_c$ on hole concentration and low carrier density. A tilt grain boundary is built of a chain of edge dislocations spaced by $d = b/2\sin(\theta/2)$, where

$b \approx 0.4$ nm is the Burgers vector. As the misorientation angle $\theta$ increases, the spacing between the insulating dislocation cores decreases, becoming of the order of the coherence length $\xi$ at $\theta \approx 5$–$7°$. For higher angles, a grain boundary becomes a Josephson weak link, because of the local suppression of the order parameter in the current channels between the dislocations, and $J_b$ decreases exponentially with increasing $\theta$[31]. Extensive electron microscopy has established that the hole content is depressed in the vicinity of grain boundaries and that there is only partial occupancy of cations in the structural units that form the boundary[51,52].

Grain boundaries possess extra ionic charge, whose magnitude increases with increasing $\theta$ and causes hole depletion in a layer of thickness given by the Thomas-Fermi screening length $l_D \approx \xi(0)$ (Fig. 5). As a result, the grain boundary is in a locally underdoped state, the local order parameter suppression increasing as $\theta$ increases[31,52]. That is why local overdoping by partially substituting Ca for Y in YBCO (refs 53,54) is effective. Adding extra carriers to the grain boundary with Ca-doping and reducing local strains can significantly increase $J_b$ (by a factor of eight for a 24° [001] tilt boundary at 4.2 K and 0 T (ref. 53), and by a factor of three for a 7°-bicrystal at 55 K and 3 T (ref. 55)). Although overdoping ameliorates, rather than removes, the problem of current obstruction by grain boundaries in HTSs, it may certainly be useful for conductors[43–45,56,57], because the critical angle $\theta_c$ is only 2–5°.

Performance of HTS conductors in a magnetic field is determined by the nature of the vortices at the grain boundaries and their pinning interaction with structural defects, and by their magnetic interactions with strongly pinned vortices within the grains (Fig. 5). Because of the extended core of grain-boundary vortices, they are generally pinned more weakly than vortices in the grains (ref. 58, and Gurevich *et al.*, submitted), and grain boundaries become barriers to current flow because their critical current density $J_b(T,H)$ is smaller than $J_c(T,H)$ in the grains. This behaviour is clearly visible in the magneto-optical images of Fig. 6, which shows preferential flux penetration along a network of coated-conductor grain boundaries[56] having $\theta > 4°$.

The influence of misorientation is less certain for compounds other than YBCO, as all other HTS compounds are harder to grow as good films on bicrystal substrates. To first approximation, thin films of $Bi_2Sr_2CaCu_2O_x$ and Bi-2223 show similar exponential decrease of $J_b(\theta)$ (refs 59,60) to that seen for YBCO, suggesting a common mechanism for suppression of critical current on grain boundaries. Experiments on float-zone $Bi_2Sr_2CaCu_2O_x$ bicrystals indicate much weaker dependence of $J_b$ on $\theta$ than for thin films[61], but the intragranular critical current densities are so small that they might not reach the critical current density of the grain boundaries. An extensive magneto-optical study of [001] tilt, thin-film YBCO bicrystals[62] has shown that the temperature dependences of $J_c$ and $J_b$ are significantly different.

## Current percolation in polycrystals

Any conductor must be polycrystalline. All conductor materials except Nb-Ti are brittle, making cracks endemic in $Nb_3Sn$, $MgB_2$, Bi-2223 and YBCO. In addition, the last three compounds all are prone to porosity. The net result is that current percolates through a polycrystalline network containing many obstructions, some of which partially block the current while others result in a total block[23]. Thus the local fraction of current-carrying cross-section is significantly less than unity. Magneto-optical imaging is an effective method of visualizing non-uniformities of current flow in polycrystalline conductor forms, as shown in Fig. 7 for $MgB_2$, Bi-2223 and YBCO. These images show the 'roof' pattern of the perpendicular magnetic field, resulting from screening currents induced by an external field. For $MgB_2$ the finest, visible-scale variation seems to be controlled by ~10% porosity[63] and not by grain boundaries[17,20,64]. For the Bi-2223 tape, a transverse feathering of the image is caused principally by quasiperiodic fluctuations of the superconductor

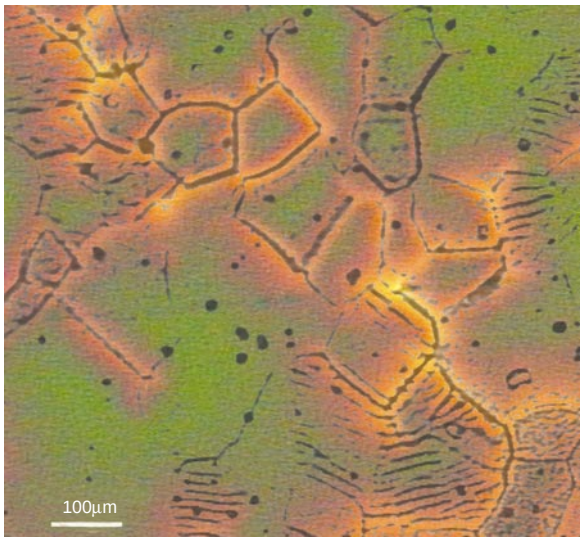


**Figure 6** Magneto-optical image of the flux penetrating into a typical deformation-textured YBCO coated conductor overlaid on a light-microscope image of the underlying Ni substrate. Darker (green) areas are regions that are well connected electromagnetically, whereas the lighter (orange) flux network indicates where the local current density is reduced. Some grain boundaries in the Ni substrate (black) do not appear in the magneto-optical image. However, all grain boundaries with misorientations greater than 4° do appear[56].

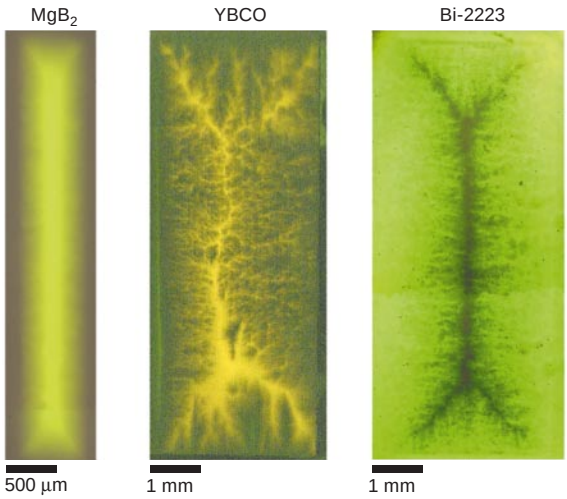


**Figure 7** Magneto-optical images of (left to right) a sintered $MgB_2$ slab[63], a YBCO IBAD-coated conductor, and a Bi-2223 monocore tape[23]. Each tape shows a global roof-top pattern of the perpendicular component of magnetic field above the superconductor surface. This 'rooftop' pattern arises from induced magnetization currents circulating through the entire sample. The $MgB_2$ slab shows the most uniform current flow, even though it is imaged in an applied field of zero after cooling in 120 mT to 37 K, only 2 K below $T_c$. Almost no spatial variation of $J_c$ is visible. The coated conductor was imaged after field-cooling in 60 mT to 11 K, well below its $T_c$ of 90 K, then reducing the applied field to zero. The Bi-2223 tape was imaged at 11 K after cooling without field and then applying a filed of 120 mT. Some feathering of the image transverse to the tape length indicates a longitudinal variation of the current, probably associated with rolling defects.

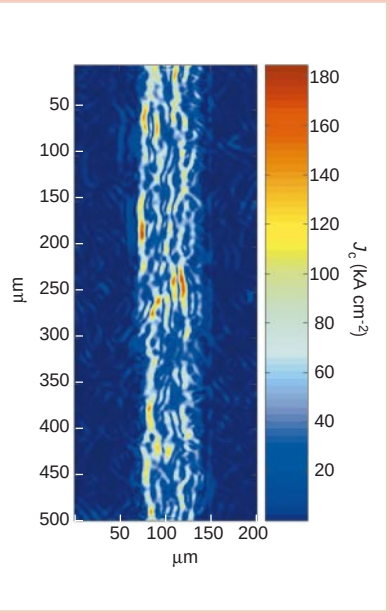


**Figure 8** Colour map of the spatial distribution of the local critical current density in the same monocore Bi-2223 tape imaged in Fig. 7. The tape was imaged in a slab geometry produced by sectioning the tape along a centre line parallel to the tape length. The image from which the current reconstruction was performed was made by cooling the slab to 77 K in zero field, then applying a field of 36 mT parallel to the half width of the slab. The transport critical current density $J_c$(77K,0T) of the tape was 35 kA cm$^{-2}$, about the median of the distribution seen in the $J_c$ map. Peak values of the $J_c$ exceeded 180 kA cm$^{-2}$.

thickness and residual rolling damage[23]. For the YBCO-coated conductor, there are multiple lines emanating from the central roof pattern, indicating local, higher current density loops superimposed upon the long-range current. Thus magneto-optical examination shows explicitly that there are multiple scales of current loops flowing in polycrystalline HTS samples. Such images pose the question: by how much is the average current density — defined by $J_c = I_c/A$, where $A$ is the total cross-section, rather than the active cross-section $A_{effective}$ — reduced below the flux-pinning critical current density established within each grain?

To answer such a question requires good understanding of the intragrain critical current densities. In fact, the magnitude of the intragrain $J_c$ of Bi-2223 remains unclear, because few high-quality bulk or thin-film single crystals have been made. Several thin-film results[38,60] suggest that $J_c$(77K,0T) can achieve 1 MA cm$^{-2}$, whereas a single-crystal study[65] gave $J_c$ values significantly less than $10^5$ A cm$^{-2}$. At 77 K and 0 T, Bi-2223 conductors can achieve up to ~75 kA cm$^{-2}$ for small current conductors[66] and 40–50 kA cm$^{-2}$ for high current conductors having $I_c$ ~150 A (refs 19,67). Figure 8 shows the results of a recent magneto-optical current reconstruction[23] on a high-$J_c$ monofilament conductor with $J_c$(77K,0T) = 35 kA cm$^{-2}$. Remarkably, $J_c$ can achieve local values of 180 kA cm$^{-2}$, up to five times higher than the transport $J_c$. Although there is a tendency for the highest-$J_c$ regions to be located at the Ag–superconductor interface, in fact very-high-$J_c$ regions are located throughout the tape. Such local variability is not surprising for a seven-component system, because it is hard to control the phase-conversion reaction of $Bi_2Sr_2CaCu_2O_x$ and other constituents to Bi-2223. Images such as Fig. 8 offer the possibility of directly correlating the local microstructure to the local $J_c$. It is interesting to note that regions of $J_c$ exceeding 100 kA cm$^{-2}$ are 50–100 μm long, several times the ~20-μm grain length. Although earlier work[68] suggested that high-$J_c$ regions were confined mainly to the Ag interface region, more recent results show that better processing is producing much more uniform $J_c$ distribution across Bi-2223/Ag tapes, resulting in significant gains in tape performance.

State-of-the-art Bi-2223 conductors contain grains ~20 μm long by ~1 μm thick, distributed in 30–60 filaments, each of which is of the order of 5–10 μm thick by 200–300 μm wide. The current percolates in a three-dimensional manner through a polycrystalline array, which possesses a significant *c*-axis texture, of the order of 10–12° full-width at half-maximum (FWHM), but has little in-plane texture. By contrast, YBCO-coated conductors rely on epitaxy and are controlled mostly by the two-dimensional percolation[69,70]. Figure 9 images the local field produced by current flowing along a track in a representative coated conductor. An extended planar array of misoriented grains obstructs the current, forcing it to flow non-uniformly and causing local dissipation, even at $0.5I_c$, where, as usual, $I_c$ is defined at the electric field criterion of 1 μV cm$^{-1}$ established across the whole track. As $I$ increases, the current-obstructing network expands, eventually becoming continuous across the whole conductor. Such images show that $I_c$ is determined locally, with many regions of the sample showing no signs of dissipation even at $I = 1.5I_c$. A similar conductor had a global $J_c$(77K,0T) of 1.2 MA cm$^{-2}$, but individual clusters of YBCO grains had $J_c$ values[57] exceeding 5 MA cm$^{-2}$. Thus, even in the biaxially textured coated conductors for which both in- and out-of-plane texture FWHM values are significantly below 10°, there is abundant evidence for current percolation around a network of obstructing grain boundaries and other defects.

Present $J_c$(77K,0T) values in 1–2-cm-long coated conductor prototypes[71–74] typically fall in the range 1–3 MA cm$^{-2}$. Further performance improvement may be impeded by electromagnetic and thermal instabilities, such as flux jumping, hot-spot formation and quench propagation, the same factors which limit the current-carrying capability of low-$T_c$ superconductors[9,75]. Whatever future microstructure improvements occur, current-obstructing obstacles are inevitable in any practical long-length forms. Because the electromagnetic and thermal stability of the current-carrying state is influenced by hot spots near obstacles, the architecture of coated

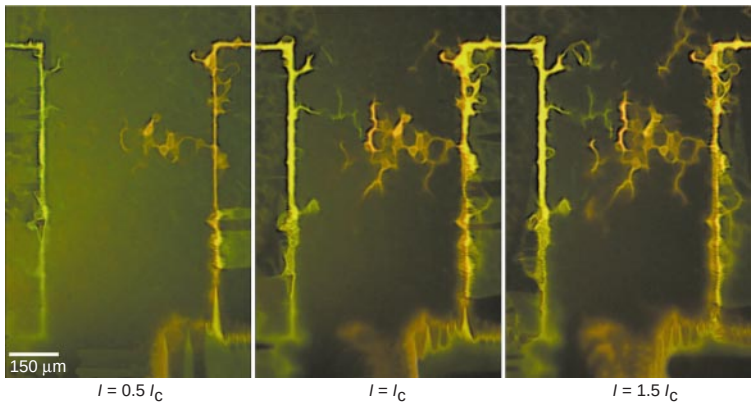


**Figure 9** Magneto-optical images at 77 K of the self-field produced by an applied transport current in a RABiTS coated conductor sample for which the full-width $J_c$(77K,0T) was 0.7 MA cm$^{-2}$. A laser was used to cut a link restricting the current flow to a region 0.5 × 1.1 mm, which had a $J_c$(77K,0T) of 0.6 MA cm$^{-2}$. Images shown are at applied currents for the link of (left to right) $0.5I_c$, $I_c$, and $1.5I_c$, where $I_c$ is defined at 1 μV cm$^{-1}$. A cluster of YBCO grain boundaries is visible in all the images, indicating where in the link $J_c$ is limited well before the onset of bulk dissipation. As the current is increased, percolation near the visible cluster of grain boundaries becomes more pronounced, but above and below this cluster current flows more uniformly, and preferentially near the edges of the link. Even at $1.5I_c$, much of the link is supporting a current less than its local $J_c$. Patterning of bridges has shown that the intragrain $J_c$ can reach 5 MA cm$^{-2}$, several times the $J_c$ of this bridge. It is clear that current is percolating through a network of grain boundaries, which also result in localized dissipation in the track.

conductors needs to be optimized so as to reduce local dissipation by current redistribution to the Ag stabilizer, and enhance heat transfer from the YBCO to the coolant. An important question is what is the acceptable size and concentration of obstructive hot spots, which provides stable conductor operation.

Because obstructions initiate dissipation, the spatial distribution of the electric field $E(x,y)$ near such obstructions controls the $I_c$ of the conductor. But unlike current distributions, which can be extracted from magneto-optical images, the electric field distribution is much harder to measure. Recently, analytical methods for the calculation of $E(x,y)$, taking account of the highly nonlinear $E$–$J$ characteristic of a superconductor, have been developed[76,77]. For $J < J_c$, the $E$–$J$ relation is determined by thermally activated flux creep, which is conventionally approximated as $E = E_c(J/J_c)^n$, where $E_c \sim 1\ \mu V\ cm^{-1}$, and the exponent $n(T,H)$ varies from 20–30 for $H << H^*$ to $n \approx 1$ at $H = H^*$. Calculations for a planar defect perpendicular to current flow show that the nonlinearity of $E(J)$ strongly enhances the electric field in extended regions of length $L_\perp \sim na$ perpendicular to the current, on a scale much larger than the defect size $a$. This behaviour is in stark contrast to ohmic conductors, in which current flow becomes essentially uniform at a distance $\sim a$ away from the defect. These long-range disturbances of $E(x,y)$ become particularly important in a coated conductor, because even a small defect can produce a large hot spot that spans the entire conductor if $a > d/n$, where $d$ is the sample width. If this rather weak condition is satisfied (typically, $n \sim 20$–30 in HTSs), then even small defects produce significant local excess dissipation. Figure 10 shows the calculated distribution of the electric field near a planar defect of length $a = 0.1d$ and $n = 20$. Even for such a small defect, the disturbance of $E(x,y)$ is much stronger than the applied field $E_0$ and extends all the way to the opposite side of the film[77].

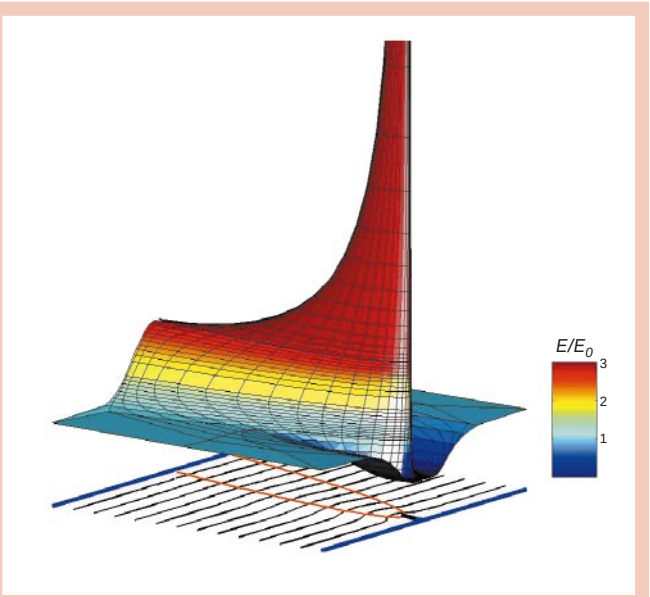


**Figure 10** Spatial distribution of the electric field $E(x,y)$ for the power-law $E$–$J$ characteristic, $E = E_c(J/J_c)^n$, near a planar defect of length $a$ in a film of width $d$, $n = 20$ and $a = 0.1d$, as calculated in refs 76,77. The lower part of the figure shows the current streamlines (black) and the boundaries (red) of the hot spot of strongly enhanced electric field lying in the film plane. It is clear that even a small defect produces the extended hot spot that effectively blocks the entire cross-section and can result in thermal instabilities[75].

## Materials fabrication considerations

One of our fundamental conclusions is that both Bi-2223 and YBCO fulfil the essential requirements for wide applications of superconductivity in the electric utility network. Conductors of Bi-2223 (and $Bi_2Sr_2CaCu_2O_x$) are available today from several companies for service in 'real-world' utility sites. Cost and performance are not yet as good as are needed for widespread substitution of copper and iron, but significant special applications exist even at much higher costs. A key question for a cost-sensitive market for HTSs is to understand how much residual $J_c$ performance capability there is in the materials themselves. As we have emphasized, the intragrain $J_c$ capability of both Bi-2223 and YBCO is several times higher than realized in today's conductors. Material defects control the overall critical current density of present conductors and these defects are intimately tied to their particular fabrication processes. Although the specifics of particular fabrication processes are beyond the scope of this article, certain general points can be made to emphasize the decisive role that materials engineering now must play in developing this technology.

As Figure 1 shows, four of the five conductors are made by conventional composite metal-working techniques. A merit of conventional metal working is that there is little conceptual barrier to scale-up. Making longer wires is mostly a question of starting with larger pieces and using larger equipment. Both $MgB_2$ and Bi-2223 wires or tapes use essentially the same technology as that used for $Nb_3Sn$ powder-in-tube composites. In fact, there is now no fundamental barrier to the production of a kilometre-long $MgB_2$ wire, and many groups have already demonstrated powder-in-tube conductors[30,78–82]. What is less clear is how much of a niche there is for $MgB_2$ to fill, because even in its high resistivity form which maximizes the upper critical field[17] it seems that the perpendicular irreversibility field is less than for $Nb_3Sn$. This is likely to restrict $MgB_2$ to applications of lower field, say 2-3 T, where the ability to operate at ~20 K is decisive economically[13]. By contrast, it has proven hard to scale up the YBCO-coated conductor to a genuinely continuous process, even after multiple proofs of principle have shown that an appropriate substrate–buffer–YBCO architecture can be made by physical vapour deposition and/or chemical methods[71–74,83]. The key issue here is to understand the defect populations that are characteristic of each fabrication method, and the capability and cost associated with reducing them to tolerable levels.

In assessing progress on HTS conductors, it is particularly relevant to recall that $Nb_3Sn$ is now celebrating 40 years as a conductor and is still improving[84,85]. Bi-2223 has had 10 years of industrial development and is also still developing strongly in attaining higher current density, reducing cost and in becoming more mechanically robust[86–88]. The complexity of its microstructure and the interactions between fabrication and basic materials issues is slowly becoming clear[89], not least because multiple companies worldwide are selling the conductor in competition with each other. As Fig. 8 shows, the key issue is to increase the connectivity of the conductor. The prospect of two- to fivefold improvements in the performance of the present process, coupled to cost reductions triggered by significant scale-up and alternative routes such as overpressure processing[90] or melt processing[91], could accelerate the early penetration of superconducting technology into the utility network. At the same time, this would provide time and rationale for solving the complex issues associated with scale-up of the YBCO coated conductors.

Any manufacturing method for YBCO conductors relies on the epitaxial deposition of YBCO onto a textured template of one or more oxide buffer layers and a normal metal substrate. This template is usually created through introduction of texture either into the buffer layers by ion beam-assisted deposition (IBAD)[47], or into the metal substrate by deformation texturing using the rolling-assisted biaxially textured substrate (RABiTS)[46] approach. The IBAD method enables the use of strong, non-magnetic Ni-superalloy substrates on which an IBAD of aligned YSZ is deposited. This process can achieve a high degree of texture with a layer of YSZ that is ~0.5 μm thick. But such a process is widely considered to be too slow to be commercial. IBAD of MgO produces good texture within the first 1-2 nm and thus may be rapid enough to be commercial[92], but the degree of texture in

present IBAD-MgO-coated conductors is not yet as good as in IBAD-YSZ variants[93]. The inclined substrate deposition (ISD)[94] process is much quicker than IBAD, but the texture is significantly worse[95]. Ion-texturing processes for buffer-layer deposition[96] are receiving renewed attention owing to their simplicity, but their success depends on producing sufficient texture so to compete with the slower and more expensive IBAD process.

All of these methods of producing a textured buffer layer involve physical vapour-deposition processes, which some believe are inherently too expensive for copper and iron replacement[71]. An advantage of the RABiTS approach is that all buffer-layer and YBCO-coating steps can be performed with non-vacuum processes. A strong [100] cube texture is introduced into the substrate by conventional rolling and recrystallization[46]. Although the RABiTS approach has been developed mainly with pure Ni, alloyed substrate materials are being developed to increase the strength and reduce the magnetism of the Ni.

At this stage it is not at all clear which route to a coated conductor will win out. The design of a coated conductor is such that a substrate thickness of ~50 μm is needed to support 1–5 μm of YBCO, giving a superconductor fraction of ~5–10%, compared with the 25–50% for conductors made by metal-working techniques. Short samples of both IBAD and RABiTS conductors can both exceed 2 MA $cm^{-2}$ for YBCO layers up to ~0.5 μm. But thicker YBCO layers tend to exhibit less epitaxy, more porosity and thus smaller $J_c$. Degradation of the $J_c$ of the YBCO layer as it grows is a serious and poorly understood problem. The principal cause seems to be loss of epitaxy once the layer gets thicker than ~0.5 μm. A proper understanding is required, as virtually all growth methods except liquid-phase epitaxy seem to share this degradation.

## Summary

The fundamental crystal and electronic structure of superconductors determines their structural anisotropy and superconducting properties. Generally, the higher the value of $T_c$, the higher the anisotropy, and the greater the upper critical field and sensitivity to nanoscale variations of the superconducting properties. This variation is positive in the case of point and line defects, because it can lead to strong flux-pinning and high critical current density. The low carrier density, short coherence length, d-wave pairing symmetry and proximity to the metal–insulator transition of HTSs makes interfaces such as grain boundaries significant barriers to current flow, except at very small misorientations. In the higher carrier density LTS materials such as Nb-Ti, $Nb_3Sn$, and $MgB_2$, grain boundaries act as beneficial flux-pinning sites without being barriers to current flow.

Anisotropy exerts two additional, important influences on conductor design, and causes significant suppression of $H^*$ as compared to $H_{c2}$. $MgB_2$, YBCO and Bi-2223 all exhibit higher critical current density, irreversibility field and upper critical field when the magnetic field is applied parallel to their layered structure. But in practice, either because of the inevitable misalignments that are present in any real wire or because the magnetic field cannot always be arranged to be parallel to the layers, it is the poorer perpendicular properties that generally control performance. An additional burden for YBCO and Bi-2223 is that the grain-to-grain misalignment must be held to values of 5° or less if obstruction of current across the grain boundaries is to be minimized. Thus planar conductor forms, which confer texture, are preferred.

These fundamental materials issues restrict the fabrication technologies available for conductors. So far all three industrially available conductors, Nb-Ti, $Nb_3Sn$ and Bi-2223, use composite metal-working techniques, which are relatively easy to scale up from laboratory to factory. It is already clear that this technique will work too for $MgB_2$. But it does not work for YBCO, for which a multilayer epitaxial technique is required. Many techniques using a variety of chemical and physical vapour-deposition techniques can be used to make short samples that demonstrate the concept of the coated conductor. At present the coated conductor R&D community is attempting to work out which fabrication techniques work cost-effectively in continuous processes. Broad and significant applications exist and await only the resolution of the vital materials issues that control development of the cheap, high-performance conductor-fabrication technology that underpins all superconducting applications. □


1. Berlincourt, T. G. Type-II superconductivity: quest for understanding. *IEEE Trans. Magn.* **23,** 403–412 (1987).
2. Kunzler, J. E., Buehler, E., Hsu, L. & Wernick, J. Superconductivity in $Nb_3Sn$ at high current density in a magnetic field of 88 kgauss. *Phys. Rev. Lett.* **6,** 89–91 (1961).
3. Gavaler, J. Superconductivity in Nb-Ge films above 22 K. *Appl. Phys. Lett.* **23,** 480–482 (1973).
4. Bednorz, G. & Muller, K. A. Possible high-$T_c$ superconductivity in the Ba-La-Cu-O system. *Z. Phys. B* **64,** 189–193 (1986).
5. Wu, M. K. *et al.* Superconductivity at 93 K in an new mixed-phase Y-Ba-Cu-O compound system at ambient pressure. *Phys. Rev. Lett.* **58,** 908–912 (1987).
6. Schilling, A., Cantoni, M., Guo, J. D. & Ott, H. R. Superconductivity above 130 K in the Hg-Ba-Ca-Cu-O system. *Nature* **363,** 56–58 (1993).
7. Larbalestier, D. C. *et al.* Power Applications of Superconductivity in Japan and Germany (World Technology and Engineering Center, Loyola College, MD, September 1997).
8. Nagamatsu, J., Nakagawa, N., Muranaka, T., Zenitani, Y. & Akimitsu, J. Superconductivity at 39 K in magnesium diboride. *Nature* **410,** 63–64 (2001).
9. Wilson, M. *Superconducting Magnets* (Clarendon, Oxford, 1983).
10. Dew-Hughes, D. *Physics and Materials Science of Vortex States, Flux Pinning and Dynamics* NATO Science Ser. E, Vol. 356 (eds Kossowsky, R., Bose, S., Pan, V. & Durosoy, Z.) 705–730 (Kluwer Academic, Dordrecht, 1999).
11. Hassenzahl, W. V. Superconductivity, an enabling technology for 21st century power systems? *IEEE Trans. Appl. Supercond.* **11,** 1447–1453 (2001).
12. Radebaugh, R. in *Advances in Cryogenic Engineering* Vol. 44 (eds Haruyama, T., Mitsui, T. & Yamafuji, K.) 33–44 (Elsevier Science, 1997).
13. Grant, P. Rehearsals for prime time. *Nature* **411,** 532–533 (2001).
14. Suenaga, M., Ghosh, A. K., Hu, Y. & Welch, D. O. Irreversibility temperatures of $Nb_3Sn$ and Nb-Ti. *Phys. Rev. Lett.* **66,** 1777–1780 (1991).
15. Brandt, E. H. The flux line lattice in superconductors. *Rep. Prog. Phys.* **58,** 1465–1594 (1995).
16. Xu, M. *et al.* Single crystal $MgB_2$ with anisotropic superconducting properties. Preprint cond-mat/0105271 at <http://xxx.lanl.gov> (2001).
17. Patnaik, S. *et al.* Electronic anisotropy, magnetic field-temperature phase diagram and their dependence on resistivity in c-axis oriented $MgB_2$ thin films. *Supercond. Sci. Technol.* **14,** 315–319 (2001).
18. Blatter, G., Feigelman, M. V., Geshkenbein, V. B., Larkin, A. I. & Vinokur, V. M. Vortices in high-temperature superconductors. *Rev. Mod. Phys.* **66,** 1125–1388 (1994).
19. Schwartzkopf, L. A., Jiang, J., Cai, X. Y., Apodaca, D. & Larbalestier, D. C. The use of the in-field critical current density, $J_c$(0.1T), as a better descriptor of $(Bi,Pb)_2Sr_2Ca_2Cu_3O_x$/Ag tape performance. *Appl. Phys. Lett.* **75,** 3168–3170 (1999).
20. Canfield, P. C. *et al.* Superconductivity in dense $MgB_2$ wires. *Phys. Rev. Lett.* **86,** 2423–2426 (2001).
21. Tinkham, M. *Introduction to Superconductivity.* (McGraw Hill, New York, 1975).
22. Campbell, A. M. & Evetts, J. E. Flux vortices and transport current in type-II superconductors. *Adv. Phys.* **21,** 194–428 (1972).
23. Polyanskii, A. A. *et al.* Examination of current limiting mechanisms in monocore Ag/BSCCO tape with high critical current density. *IEEE Trans. Appl. Supercond.* **11,** 3269–3270 (2001).
24. Meingast, C. & Larbalestier, D. C. Quantitative description of a very high critical current density Nb-Ti superconductor during its final optimization strain. II. Flux pinning mechanisms. *J. Appl. Phys.* **66,** 5971–5983 (1989).
25. Kramer, E. J. Dynamics of dislocation dipole motion in the flux line lattice of type-II superconductors. *J. Appl. Phys.* **41,** 621–629 (1970).
26. Dew-Hughes, D. The role of grain boundaries in determining $J_c$ in high-field, high current superconductors. *Phil. Mag.* **55,** 459–449 (1987).
27. Cooley, L. D., Lee, P. J. & Larbalestier, D. C. Changes in flux pinning curve shape for flux-line separations comparable to grain size in $Nb_3Sn$ wires. *Adv. Cryo. Eng.* (in the press).
28. Eom, C. B. *et al.* High critical current density and enhanced irreversibility field in superconducting $MgB_2$ thin films. *Nature* **411,** 558–560 (2001).
29. Song, X. *et al.* Anisotropic grain morphology, crystallographic texture and their implications for the electromagnetic properties of polycrystalline $MgB_2$ thin films, sintered pellets and filaments. *Supercond. Sci. Technol.* (in the press).
30. Jin, S., Mavoori, H., Bower, C. & van Dover, R. B. High critical current in iron-clad superconducting $MgB_2$ wires. *Nature* **411,** 563–565 (2001).
31. Gurevich, A. & Pashitskii, E. A. Current transport through low-angle grain boundaries in high-temperature superconductors. *Phys. Rev. B* **57,** 13878–13893 (1998).
32. Pan, S. H. *et al.* Imaging the effect of individual zinc impurities on superconductivity in $Bi_2Sr_2CaCu_2O_{8+\delta}$. *Nature* **403,** 746–750 (2000).
33. Pan, S. H. *et al.* Microscopic electronic inhomogeneity in the high-$T_c$ superconductor $Bi_2Sr_2CaCu_2O_{8+x}$. *Nature* **413,** 282–285 (2001).
34. Kes, P. Flux pinning and creep in high-temperature superconductors. *Physica C* **185,** 288–291 (1991).
35. Diaz, A., Mechin, L., Berghuis, P. & Evetts, J. E. Evidence for vortex pinning by dislocations in $YBa_2Cu_3O_7$ low angle grain boundaries. *Phys. Rev. Lett.* **80,** 3855–3858 (1998).
36. Dam, B. *et al.* Origin of high critical currents in $YBa_2Cu_3O_7$ superconducting thin films. *Nature* **399,** 439–442 (1999).
37. Hilgenkamp, H. & Mannhart, J. Grain boundaries in high-Tc superconductors. *Rev. Mod. Phys.* (in the press).
38. Miu, L. *et al.* Vortex unbinding and layer decoupling in epitaxial $Bi_2Sr_2Ca_2Cu_3O_{8+\delta}$ films. *Phys. Rev. B* **52,** 4553–4558 (1995).
39. Vargas, J. L. & Larbalestier, D. C. Flux pinning by ordered oxygen deficient phases in nearly stoichiometric $YBa_2Cu_3O_{7-\delta}$ single crystals. *Appl. Phys. Lett.* **60,** 1741–1743 (1992).

40. Yeshurun, Y., Malozemoff, A. P. & Shaulov, A. Magnetic relaxation in high-temperature superconductors. *Rev. Mod. Phys.* **68,** 911–949 (1996).
41. Civale, L. Vortex pinning and creep in superconductors with columnar defects. *Supercond. Sci. Technol.* **10,** A11–A28 (1997).
42. Tonies, S. *et al.* On the current transport limitations in Bi-based high temperature superconducting tapes. *Appl. Phys. Lett.* **78,** 3851–3853 (2001).
43. Dimos, D., Chaudhari, P. & Mannhart, J. Superconducting transport properties in $YBa_2Cu_3O_{7-\delta}$ bicrystals. *Phys. Rev. B* **41,** 4038–4049 (1990).
44. Heinig, N. F., Redwing, R. D., Nordman, J. E. & Larbalestier, D. C. Strong to weak coupling transition in low misorientation angle thin film $YBa_2Cu_3O_{7-\delta}$ bicrystals. *Phys. Rev. B* **60,** 1409–1417 (1999).
45. Verebelyi, D. *et al.* Low angle grain boundary transport in $YBa_2Cu_3O_{7-\delta}$ coated conductors. *Appl. Phys. Lett.* **76,** 1755–1757 (2000).
46. Goyal, A. *et al.* Texture formation and grain boundary network in rolling assisted biaxially textured substrates and in epitaxial YBCO films. *Micron* **30,** 463–478 (1999).
47. Iijima, Y., Kakimoto, K., Kimura, M., Takeda, K. & Saitoh T. Reel to reel continuous formation of Y-123 coated conductors by IBAD and PLD method. *IEEE Trans. Appl. Supercond.* **11,** 2816–2821 (2001).
48. Larbalestier, D. C. & West, A. W. New perspective on flux pinning in niobium-titanium composite superconductors. *Acta Metall.* **32,** 1871–1881 (1984).
49. Cooley, L. D., Daeumling, M., Willis, T. W. & Larbalestier, D. C. Weak link behavior in polycrystalline $BaPb_{0.75}Bi_{0.25}O_3$. *IEEE Trans. Magn.* **25,** 2314–2316 (1989).
50. Takagi, T., Chiang, Y. M. & Roshko, A. Origin of grain-boundary weak links in $BaPb_{1-x}Bi_xO_3$ superconductor. *J. Appl. Phys.* **68,** 5750–5758 (1990).
51. Babcock, S. E. & Vargas, J. L. The nature of grain boundaries in high-$T_c$ superconductors. *Annu. Rev. Mater. Sci.* **25,** 193–222 (1995).
52. Browning, N. D. *et al.* The atomic origin of reduced critical currents at [001] tilt grain boundaries in $YBa_2Cu_3O_7$ thin films. *Physica C* **294,** 183–193 (1998).
53. Schmehl, A. *et al.* Doping induced enhancement of the critical currents of grain boundaries in $YBa_2Cu_3O_7$. *Europhys. Lett.* **47,** 110–115 (1999).
54. Hammerl, G. *et al.* Enhanced supercurrent density in polycrystalline $YBa_2Cu_3O_7$ at 77K from calcium doping of grain boundaries. *Nature* **407,** 162–164 (2000).
55. Daniels, G. A., Gurevich, A. & Larbalestier, D. C. Improved strong magnetic field performance of low angle grain boundaries of calcium and oxygen overdoped $YBa_2Cu_3O_7$. *Appl. Phys. Lett.* **77,** 3251–3253 (2000).
56. Feldmann, D. M. *et al.* Influence of nickel substrate grain structure on $YBa_2Cu_3O_7$ supercurrent connectivity in deformation-textured coated conductors. *Appl. Phys. Lett.* **77,** 2906–2908 (2000).
57. Feldmann, D. M. *et al.* Inter and intra-grain transport measurements in $YBa_2Cu_3O_{7-x}$ deformation textured coated conductors. *Appl. Phys. Lett.* (in the press).
58. Gurevich, A. & Cooley, L. D. Anisotropic flux pinning in a network of planar defects. *Phys. Rev. B* **50,** 13563–13576 (1994).
59. Amrein, T., Schultz, L., Kabius, B. & Urban, K. Orientation dependence of grain boundary critical current in high-$T_c$ bicrystals. *Phys. Rev. B* **51,** 6792 (1995).
60. Attenberger, A. *Electrische transportmessungen uber definierte Korngrenzen-Strukturen in epitaktischen Bi-2223 Schichten*. Thesis, Technische Universitat Dresden (2000).
61. Tsay, Y. N. *et al.* Transport properties of $Bi_2Sr_2CaCu_2O_{8+\delta}$ bicrystals with [001] tilt grain boundaries. *IEEE Trans. Appl. Supercond.* **9,** 1622–1625 (1999).
62. Polyanskii, A. A. *et al.* Magneto-optical study of flux penetration and critical current densities in [001] tilt $YBa_2Cu_3O_7$ thin-film bicrystals. *Phys. Rev. B* **53,** 8687–8697 (1996).
63. Polyanskii, A. A. *et al.* Magneto-optical studies of the uniform critical state in bulk $MgB_2$. *Supercond. Sci. Technol.* **14,** 811–815 (2001).
64. Larbalestier, D. C. *et al.* Strongly linked current flow in polycrystalline forms of the superconducting $MgB_2$. *Nature* **410,** 186–189 (2001).
65. Chu, S. Y. & McHenry, M. E. Growth and characterization of $(Bi,Pb)_2Sr_2Ca_2Cu_3O_x$ single crystals. *J. Mat. Res.* **13,** 589–595 (1998).
66. Malozemoff, A. P. *et al.* HTS wires at commercial performance levels. *IEEE Trans. Appl. Supercond.* **9,** 2469–2473 (1999).
67. Huang, Y. B. *et al.* Progress in Bi-2223 tape performance. *Adv. Cryo. Eng.* (in the press).
68. Pashitski, A. E., Polyanskii, A., Gurevich, A., Parrell, J. A. & Larbalestier, D. C. Magnetic granularity, percolation and preferential current flow in a silver-sheathed $Bi_{1.8}Pb_{0.4}Sr_2Ca_2Cu_3O_{8+x}$ tape. *Physica C* **246,** 133 (1995).
69. Holzapfel, B. *et al.* Grain boundary networks in Y123 coated conductors. Formation, properties and simulation. *IEEE Trans. Appl. Supercond.* **11,** 3872–3875 (2001).
70. Rutter, N. & Glowacki, B. Modelling of orientation relations in 2-D percolative systems of buffered metallic substrates for coated conductors. *IEEE Trans. Appl. Supercond.* **11,** 2730–2733 (2001).
71. Rupich, M. W. *et al.* Low cost Y-Ba-Cu-O coated conductors. *IEEE Trans. Appl. Supercond.* **11,** 2927–2930 (2001).
72. Maeda, T. *et al.* $YBa_2Cu_3O_x$ thick films grown on textured metal substrates by liquid-phase epitaxy process. *IEEE Trans. Appl. Supercond.* **11,** 2931–2934 (2001).
73. Solovyov, V. *et al.* Ex situ post-deposition processing for large area $YBa_2Cu_3O_x$ films and coated tapes. *IEEE Trans. Appl. Supercond.* **11,** 2939–2943 (2001).
74. Holesinger, T. *et al.* A comparison of buffer layer architectures on continuously processed YBCO coated conductors based on the IBAD YSZ process. *IEEE Trans. Appl. Supercond.* **11,** 3359–3364 (2001).
75. Gurevich, A. Thermal instability near planar defects in superconductors. *Appl. Phys. Lett.* **78,** 1891–1893 (2001).
76. Gurevich, A. & Friesen, M. Nonlinear current flow in superconductors with planar obstacles. *Phys. Rev. B* **62,** 4004–2025 (2000).
77. Friesen, M. & Gurevich, A. Nonlinear current flow in superconductors with restricted geometries. *Phys. Rev. B* **63,** 064521-1-26 (2001).
78. Glowacki, B. A. *et al.* Superconductivity of powder-in-tube $MgB_2$ wires. *Supercond. Sci. Technol.* **14,** 193–199 (2001).
79. Suo, H. L. *et al.* High transport and inductive critical currents in dense Fe- and Ni-clad $MgB_2$ tapes using fine powder. *Adv. Cryo. Eng.* (in the press).
80. Grasso, G. *et al.* Preperation and properties of unsintered $MgB_2$ supercondcuting tapes. *Adv. Cryo. Eng.* (in the press).
81. Kumakura, H., Matsumoto, A., Fujii, H., Takano, Y. & Togano, K. Fabrication and superconducting properties of powder-in-tube processed $MgB_2$ tapes and wires. *Adv. Cryo. Eng.* (in the press).
82. Grasso, G. *et al.* Large transport critical currents in unsintered $MgB_2$ superconducting tapes. *Appl. Phys. Lett.* **79,** 230–232 (2001).
83. Malozemoff, A. P. *et al.* D. F. Low-cost YBCO coated conductor technology. *Supercond. Sci. Technol.* **13,** 473–476 (2000).
84. Pyon, T. & Gregory, E. $Nb_3Sn$ conductors for high energy physics and fusion applications. *IEEE Trans. Appl. Supercond.* **11,** 3688–3691 (2001).
85. Field, M., Hentges, R., Parrell, J., Zhang, Y. & Hong, S. Progress with $Nb_3Sn$ conductors at Oxford Instruments–Superconducting Technology. *IEEE Trans. Appl. Supercond.* **11,** 3692–3695 (2001).
86. Wang, W. G. *et al.* Engineering critical current density improvement in Ag-Bi-2223 tapes. *IEEE Trans. Appl. Supercond.* **11,** 2983–2986 (2001).
87. Masur, L. *et al.* Long length manufacturing of high performance BSCCO-2223 tape for the Detroit-Edison Power Cable Project. *IEEE Trans. Appl. Supercond.* **11,** 3256–3260 (2001).
88. Hayashi, K. *et al.* Development of Ag-sheathed Bi2223 superconducting wires and their applications. *IEEE Trans. Appl. Supercond.* **11,** 3281–3284 (2001).
89. Jiang, J. *et al.* Through-process study of factors controlling the critical current density of Ag-sheathed $(Bi,Pb)_2Sr_2Ca_2Cu_3O_x$ tapes. *Supercond. Sci. Technol.* **14,** 548–556 (2001).
90. Rikel, M. O. *et al.* Overpressure processing Bi2223/Ag tapes. *IEEE Trans. Appl. Supercond.* **11,** 3026–3029 (2001).
91. Flukiger, R. *et al.* Phase formation in Bi,Pb(2223) tapes. *IEEE Trans. Appl. Supercond.* **11,** 3393–3398 (2001).
92. Wang, C. P., Do, K. B., Beasley, M. R., Geballe, T. H. & Hammond, R. H. Deposition of in-plane textured MgO on amorphous $Si_3N_4$ substrates by ion-beam-assisted deposition and comparison with ion-beam-assisted deposition yttria-stabilized-zirconia. *Appl. Phys. Lett.* **71,** 2955–2957 (1997).
93. Groves, J. R. *et al.* High critical current density $YBa_2Cu_3O_{7-\delta}$ thick films using ion beam assisted deposition MgO bi-axially oriented template layers on nickel-based superalloy substrates. *J. Mater. Res.* **16,** 2175-2178 (2001).
94. Hasegawa, K. *et al.* in *Proc. 9th Int. Symp. Supercond. (IIS'96)* Vol. 2, 745–748 (Springer, Tokyo 1997).
95. Metzger, R. Superconducting tapes using ISD buffer layers produced by evaporation of MgO or reactive evaporation of magnesium. *IEEE Trans. Appl. Supercond.* **11,** 2826–2829 (2001).
96. Reade, R. P., Berdhal, P., Russo, R. E. & Garrison, S. M. Laser deposition of biaxially textured yttria-stabilized zirconia buffer layers on polycrystalline metallic alloys for high critical current Y-Ba-Cu-O thin films. *Appl. Phys. Lett.* **61,** 2231–2233 (1992).
97. Ivanov, Z. G. *et al.* Weak links and dc SQUIDS on artificial nonsymmetric grain boundaries in $YBa_2Cu_3O_{7-x}$. *Appl. Phys. Lett.* **59,** 3030 (1991).
98. Char, K. *et al.* Bi-epitaxial grain-boundary junctions in $YBa_2Cu_3O_7$. *Appl. Phys. Lett.* **59,** 733–735 (1991).



**Acknowledgements**

The authors are grateful to many colleagues for discussions and collaborations. In particular, we thank our present and former Madison colleagues S. Babcock, X. Cai, L. Cooley, G. Daniels, C.-B. Eom, E. Hellstrom, J. Jiang, P. Lee, J. Reeves, M. Rikel and X. Song, and colleagues within the Wire Development Group, especially B. Riley (AMSC), V. Maroni (ANL) and T. Holesinger (LANL). Recent collaborations on coated conductors with T. Peterson and P. Barnes (AFRL), R. Feenstra (ORNL) and D. Verebelyi (AMSC) have been particularly helpful.. R. Blaugher (NREL), G. Grasso (Genoa) and J. Mannhart (Augsburg) supplied material for the tables and figures. Finally we thank the Air Force Office of Scientific Research, the Department of Energy and the National Science Foundation for support.